Thiéry, J.M., D'Herbes, J.M. and Valentin, C., 1994. A model simulating the genesis of banding patterns in Niger. J. Ecol., accepted for publication.
Tromble, J.M., Renard, K.G. and Thatcher, A.P., 1974. Infiltration for three rangeland soil–vegetation complexes. J. Range Management, 27(4): 318–321.
Valentin, C., 1981. Organisations pelliculaires superficielles de quelques sols de région subdésertique (Agadez-Niger). Dynamique de formation et conséquences sur l'économie en eau. Thèse, Université de Paris, published in 1985. ORSTOM, Paris, Collection Etudes et Thèses, 259 pp.
Valentin, C., 1993. Soil crusting and sealing in West Africa and possible approaches to improved management. In: Soil tillage in Africa: needs and challenges, FAO, Soils Bull., 69: 95–128.
Valentin, C. and Bresson, L.M., 1992. Morphology, genesis and classification of surface crusts in loamy and sandy soils. Geoderma, 55: 225–245.
Vandervaere, J.P., Peugeot, C., Angulo Jaramillo, R., Vauclin, M. and Lebel, T., 1997. Estimating hydraulic conductivity of crusted soils by using disc infiltrometers and micro-tensiometers, this issue.
Yair, A. and Lavee, H., 1990. Runoff generation in arid and semi-arid zones. In: Anderson M.G. and Burt T.P. (Editors), Hydrological Forecasting. Wiley, Chichester, pp. 183–220.
Yair, A., Lavee, H., Bryan, R. and Adar, A., 1980. Runoff and erosion processes and rates in the Zin valley badlands, Northern Negev, Israel. Earth Surface Processes, 5: 205–225.

ELSEVIER
Journal of Hydrology 188–189 (1997) 203–223
Journal of Hydrology

Estimating hydraulic conductivity of crusted soils using disc infiltrometers and minitensiometers

J.-P. Vandervaere[a,*], C. Peugeot[a,b], M. Vauclin[a], R. Angulo Jaramillo[a], T. Lebel[a,b]

[a]Laboratoire d'étude des Transferts en Hydrologie et Environnement (LTHE, CNRS URA 1512, INPG, UJF) BP 53, 38041 Grenoble Cedex 9, France
[b]ORSTOM, laboratoire d'hydrologie, BP 5045, 34032 Montpellier Cedex, France

Abstract

Although soil crusting has long been recognized as a crucial runoff factor in the Sahel, very few field methods have been developed for the measurement of the crust hydraulic conductivity, which is difficult to achieve because of the small thickness of most surface crusts. A field method, based on the simultaneous use of disc infiltrometers and minitensiometers is proposed for determining the crust hydraulic conductivity and sorptivity near saturation. On crusted soils, the classical analysis of the steady state water flow was found to be inadequate. The proposed method is based on sorptivity measurements performed at different water supply potentials and uses recent developments of transient flow analysis. A minitensiometer, placed horizontally at the crust–subsoil interface, facilitated the analysis of the infiltration regime for the crust solely.

Results are shown for representative soil units of the East Central Super Site of the HAPEX-Sahel experiment: fallow grasslands, millet fields and tiger bush. Non-crusted soils were also considered and validated the transient method as demonstrated by comparison with Wooding's steady state solution. This validation was obtained in the case of fallow grasslands soil but not for the millet fields. In this latter case, the persistent effects of localized working of the soil to remove weeds caused large variations in infiltration fluxes between the sampling points, which tended to dominate over effects of differences in applied potential. For the tiger bush crusted soils, the ratio of the saturated hydraulic conductivity of the crust to that of the underlying soil ranges from 1/3 to 1/6, depending on whether the crust is of a structural (ST) or sedimentation (SED) type. The method also allows the estimation of a functional mean pore size, consistent with laboratory measurements, and 40% less for the crusts in comparison with the underlying soil.

The results obtained here will be used in hydrological models to predict the partition of rainfall between infiltration and runoff.

* Corresponding author.

PII S0022-1694(96)03160-5

1. Introduction

To model the interactions between the continental biosphere and the atmosphere, estimation of the water balance components requires knowledge of the hydraulic properties of the soil including the relationship between unsaturated hydraulic conductivity, K, and the soil water pressure, h, or the soil volumetric water content, θ.

Tension disc infiltrometers have become an increasingly popular device for in-situ measurement of K close to natural saturation (Clothier and White, 1981; Perroux and White, 1988; Thony et al., 1991; Mohanty et al., 1994), and papers which compare results obtained from different data analysis methods recently appeared (Hussen and Warrick, 1993; Logsdon and Jaynes, 1993; Cook and Broeren, 1994). More convenient to perform than internal drainage experiments, the methodology is an ideal tool for spatial variability studies and, additionally, it provides estimates of physical variables such as capillary sorptivity, and different characteristic time and length scales.

Based on properties of three-directional axisymmetric infiltration, most existing analytical analysis methods for disc infiltrometer data require the attainment of steady state flow, for which a simple two-term expression was found (Wooding, 1968). Assuming an exponential relationship between K and h (Gardner, 1958):

$$K = K_s \exp(\alpha H) \tag{1}$$

where K_s is the saturated hydraulic conductivity and α is a shape factor related to a functional pore size (Philip, 1987), Wooding showed that the unconfined steady state flux density averaged over a source area of radius r can be approximated by:

$$q(h_f) = K(h_f) + \frac{4\Phi(h_f)}{\pi r} \tag{2}$$

where h_f is the water pressure head at the surface ($h_f \leq 0$) and Φ is the matric flux potential defined by:

$$\Phi(h_f) = \int_{h_i}^{h_f} K(h)\mathrm{d}h \tag{3}$$

where the subscripts "i" and "f" refer to initial and boundary supply pressure conditions, respectively.

The hydraulic conductivity can thus be calculated, either by using different source radii (Scotter et al., 1982; Thony et al., 1991), or by using multiple supply potentials with the same disc (Reynolds and Elrick, 1991; Ankeny et al., 1991). However, the restrictive assumptions underlying Wooding's solution, i.e. homogeneous and isotropic soil with a uniform initial moisture content, may lead to unrealistic results including negative values of K (Hussen and Warrick, 1993; Logsdon and Jaynes, 1993).

During the HAPEX-Sahel experiment (Goutorbe et al., 1994), the main difficulty in using steady state infiltrometer methods was the presence of surface crusts which play a major role in the hydrology of the Sahelian zone as shown by many authors (Hoogmoed and Stroosnijder, 1984; Casenave and Valentin, 1989; Casenave and Valentin, 1992). Indeed, the partition between infiltration and runoff at the surface of a crusted soil depends on the hydrodynamic properties of both the crust and the underlying soil. While many attempts at quantifying the effect of a surface crust on one-dimensional infiltration have been reported (Hillel and Gardner, 1969, 1970; Ahuja, 1974; Smiles et al., 1982; Parlange et al., 1984), to our knowledge field experiments under axisymmetric flow conditions have not been performed on crusted soils. We found that classical methods of analysis applied to infiltration tests fail for crusted soils, leading to unrealistic values of K and Φ in almost all cases. Indeed, steady state infiltration into a crusted soil involves a complex combination of the hydrodynamic properties of both layers. While it is only the crust properties which play a role at early stages, the hydraulic conductivity of the crust–soil system tends to that of the subsoil at long times. Therefore, to estimate the conductivity of the crust, we developed a specific methodology using a minitensiometer placed at the crust–subsoil interface with transient flow analysis of infiltration into the crust only. The main motivation for this study is in the fact that knowledge of the hydraulic properties of both the crust and the subsoil allows the infiltration of rainfall under any conditions of intensity and duration to be modelled.

2. Theory

The proposed method is based on sorptivity determinations obtained by analyzing transient flow from disc infiltrometer experiments performed at different water supply potentials, h_f. For each test, matric flux potential is calculated from the corresponding sorptivity value and hydraulic conductivity is obtained by differentiating the matric flux potential with respect to h_f.

2.1. Transient flow and sorptivity

While one-dimensional soil infiltration is well described analytically, there were, until recently, few theoretical works on three-dimensional unconfined infiltration for a disc source. Turner and Parlange (1974) calculated an approximate analytical solution for the lateral movement at the periphery of a one-dimensional water flow. Warrick and Lomen (1976) proposed an expression for the matric flux potential as a function of time valid for a disc source and a 'α-soil', that is, described by Eq. (1). Cumulative infiltration as a function of time in axisymmetric conditions can also be predicted by numerical models (e.g. Warrick, 1992; Quadri et al., 1994) which require the complete soil hydrodynamic description. Their use with the objective to determine the soil's hydraulic conductivity through inverse procedures is thus complicated by the number of parameters to be estimated and subsequent problems dealing with possible non-uniqueness of the solution.

However, restrictions in the use of Wooding's equation, uncertainties about the time at which steady infiltration flux is attained, together with the fact that much useful information is lost by ignoring the transient stage have strengthened the need for a transient three-directional infiltration equation for disc infiltrometers. Two expressions were recently proposed for this purpose (Warrick, 1992; Haverkamp et al., 1994), having in common that the supplementary term introduced by considering unconfined edge flow is linear with time. Then, the expression of Philip (1957) for one-dimensional infiltrated depth, I_{1d}:

$$I_{1d}=S\sqrt{t}+At \tag{4}$$

where t is time, S is the capillary sorptivity, and A is a constant (LT^{-1}), is modified into:

$$I_{3d}=S\sqrt{t}+(A+B)t \tag{5}$$

where I_{3d} is the cumulative three-directional infiltrated depth and B is a constant expressed by (Haverkamp et al., 1994):

$$B=\frac{\gamma S^2}{r(\theta_f-\theta_i)} \tag{6}$$

where γ is a dimensionless constant and θ_i and θ_f are initial and final volumetric water content, respectively. Sorptivity can be determined from either non-linear fitting of Eq. (4) or Eq. (5) to field data (Bristow and Savage, 1987) or, as suggested by Smiles and Knight (1976), as the intercept of the regression of $I/\sqrt{t}$ against $\sqrt{t}$, using one of the following expressions:

$$\frac{I_{1d}}{\sqrt{t}}=S+A\sqrt{t} \tag{7a}$$

$$\frac{I_{3d}}{\sqrt{t}}=S+(A+B)\sqrt{t} \tag{7b}$$

for one- and three-dimensional cases, respectively.

To ensure the hydraulic contact between the disc infiltrometer and the soil, it is often necessary to place a fine layer of sand at the soil surface. Because of this layer, methods using cumulative data, including that of Smiles and Knight, are compromised. This is particularly the case for low permeability soils, due to the relatively large amount of water stored at early time in the sand. Indeed, taking this effect into account modifies Eq. (5) into:

$$I_{3d}=I_0+S\sqrt{(t-t_0)}+(A+B)(t-t_0) \tag{8}$$

where I_0 and t_0 are, respectively, the depth of water and the time necessary to wet the sand layer in equilibrium with h_f. Then, Eq. (7) becomes:

$$\frac{I_{3d}}{\sqrt{t}}=\frac{I_0}{\sqrt{t}}+S\sqrt{\frac{t-t_0}{t}}+(A+B)\frac{t-t_0}{\sqrt{t}} \tag{9}$$

When I_0 is large compared with S, A, and B, that is when the soil has low conductivity and sorptivity, the relationship between $I_{3d}/\sqrt{t}$ and $\sqrt{t}$ is far from linear due to the effect of the first term in the right-hand side of Eq. (9).

The influence of the sand layer is usually neglected in steady state situations and it is generally assumed that it has no effect on the final flux value. Eq. (8) shows that this influence should be taken into account for transient flow analysis, especially when a large amount of sand is applied to overcome surface roughness. Rather than analyzing cumulative infiltration data, a way to circumvent the need for I_0 is to differentiate the cumulative infiltration with respect to the square root of time. Performing this differentiation on

Eq. (5) yields:

$$\frac{\Delta I_{3d}}{\Delta\sqrt{t}}\approx\frac{\partial I_{3d}}{\partial\sqrt{t}}=S+2(A+B)\sqrt{t} \tag{10}$$

and for Eq. (8), the result is:

$$\frac{\Delta I_{3d}}{\Delta\sqrt{t}}\approx\frac{\partial I_{3d}}{\partial\sqrt{t}}=S\sqrt{\frac{t}{t-t_0}}+2(A+B)\sqrt{t} \tag{11}$$

The difference between Eqs. (9) and (11) is that the latter one is not influenced by I_0 and the correction due to t_0 quickly becomes small as time increases.

Sorptivity, initially introduced as the variable driving horizontal absorption, is commonly considered to control the early stages of vertical infiltration as well, when the effect of gravity is minor. S depends on both initial and boundary conditions. Although its exact analytical expression is not known, many approximations have been proposed (Elrick and Robin, 1981 present a review of these). White and Sully (1987) showed that S is related to the matric flux potential through the expression:

$$\Phi(h_f)=\frac{bS^2(h_i,h_f)}{(\theta_f-\theta_i)} \tag{12}$$

where b is a parameter depending on the shape of diffusivity and having a value in the range $1/2\leq b\leq\pi/4$. A reasonable intermediate value of 0.55 can be taken for most field (Smettem and Clothier, 1989) and theoretical (Warrick and Broadbridge, 1992) situations. No dependence of the b parameter on h_f was considered in our study.

2.2. *From sorptivity to conductivity*

Following Smiles and Harvey (1973), White and Perroux (1989) proposed to estimate conductivity values from sorptivity measurements performed at different supply water potentials. Indeed, Eq. (3) shows that K can be deduced by differentiation of Φ against h_f:

$$\frac{\partial\Phi}{\partial h_f}=K_f-K_i \tag{13}$$

where K_i is negligible as compared with K_f in most field situations. Combination of Eqs. (12) and (13) enables deducing K from two or more S values. To use, simultaneously, the entire set of (Φ, h_f) data obtained for each test by Eq. (12), an analytical form of the $\Phi(h_f)$ function is required. It is convenient to keep the exponential form of Eq. (1) for its ease of integration, which gives:

$$\Phi(h)=\frac{K_s}{\alpha}\exp(\alpha h) \tag{14}$$

Parlange (1972) claims that α should not be considered as a constant over the whole range of h. Thus, it is simply assumed here that variations of α with h_f are small within the range of potentials covered by the suction disc infiltrometer (typically between 0 and 150 mm of water). Moreover, it must be assumed that the decrease in α for $h\rightarrow h_i$, which is very likely, has little effect on the total area covered by Φ between h_i and h_f. This assumption is justified if the $K(h)$ function is concave upwards.

Eq. (14), which can be fitted to the experimental values for an estimation of K_s and α, has the advantage to provide, through the α parameter, an effective pore size (λ_m) from simple capillarity theory (Philip, 1987):

$$\lambda_m = \frac{\sigma\alpha}{\rho g} \tag{15}$$

where σ is surface tension, ρ is water density, and g is acceleration due to gravity.

Knowledge of sorptivity and conductivity enables estimation of t_{grav}, the time after which gravitational forces dominate capillary effects (Philip, 1969):

$$t_{grav} = \left(\frac{S}{K}\right)^2 \tag{16}$$

For $t \ll t_{grav}$, Eq. (4) can be reduced to its first term:

$$I_{1d} = S\sqrt{t} \tag{17}$$

This provides yet another sorptivity estimate, S_1, by knowing the installation depth of the minitensiometer, Z_1, and the time, t_1, at which it is reached by infiltrating water. Assuming a 'Green and Ampt' behavior, the integral defining S:

$$S = \int_{\theta_i}^{\theta_1} z(\theta) t^{-1/2} d\theta \tag{18}$$

where z is depth and θ_1 is the volumetric water content of the crust at t_1, becomes:

$$S_1 = \frac{Z_1(\theta_1 - \theta_i)}{\sqrt{t_1}} \tag{19}$$

As the infiltration is pursued long after t_1, θ_1 is not necessarily equal to θ_f measured at the end of the experiment. Indeed, the water content of the crust may still increase after t_1 and the gradient of θ behind the wetting front might be significant. Consequently, θ_1 has to be calculated from the cumulative infiltration I_1 at the instant t_1, subtracting the amount of water stored into the contact layer (estimated by knowing the volume and the porosity of the sand) and the amount of water corresponding to the edge effect (estimated by lateral wetting front measurements at t_1 and assuming a parabolic profile into the soil around the disc).

Nevertheless, the uncertainty in t_1 is the main source of poor accuracy on S_1 estimates and values calculated by Eq. (19) do not provide good estimates of Φ by Eq. (12). However, their comparison with values obtained from Eq. (11) allows any systematic bias to be checked, as well as revealing the potential for water blockage at the crust–subsoil interface.

Due to the usual difficulties in field measurements of sorptivity, little use was made of the White and Perroux (WP) method. Here, an entire set of S estimates is used to fit a single relationship between Φ and h_f, but because of the need for a same initial water content for all measurements, tests must be performed at different locations. Consequently, spatial variability of S (Talsma, 1969; Sharma et al., 1980) may require a large number of replications to obtain reliable estimates. Indeed, the slope of the $\Phi(h_f)$ relationship must be estimated with enough accuracy for the differentiation operation to be performed (see Eq. (13)). The scatter in the $\Phi(h_f)$ dataset may be important as a result of the use of squared sorptivity values.

These difficulties may explain why most of the authors have used classical steady state methods when they are applicable. It seems that only Cook and Broeren (1994) compared conductivities obtained in-situ from steady state methods with those obtained from the WP method. Thus, it appeared suitable to perform a comparison between WP and steady state approaches on non-crusted soils before applying the former one to crusted soils.

2.3. Error analysis

Logarithmic differentiation of Eq. (12) yields:

$$\frac{d\Phi}{\Phi} = \frac{db}{b} + 2\frac{dS}{S} + \frac{d\theta_f}{\theta_f} + \frac{d\theta_i}{\theta_i} \tag{20}$$

The standard error due to the use of the approximate value of 0.55 for the parameter b is difficult to estimate. The theoretical range $1/2 \le b \le \pi/4$ corresponds to a maximum error and not to a standard deviation. A value of 0.1 for the relative error of b was arbitrarily taken in this study. For each test, the error on S determination, as the intercept of the line corresponding to Eq. (11), is given by the regression analysis. The errors made on θ estimations (wet and dry weighing of samples, bulk density estimation) were found to be negligible as compared with the previous errors.

The $\log_e\Phi$ values are plotted against h_f to determine the parameters K_s and α by fitting the linearized form of Eq. (14):

$$\log_e\Phi = \log_e\left(\frac{K_s}{\alpha}\right) + \alpha h_f \tag{21}$$

For the sake of simplicity, we put:

$$\beta = \log_e\left(\frac{K_s}{\alpha}\right) \tag{22}$$

Because each point was obtained at a single spot, the errors on K_s and α due to scatter of the data account for spatial variability of soil properties, causing a location error. The linear regression analysis gives standard deviation errors, $\Delta\alpha$ and $\Delta\beta$, on the slope α and the intercept β, respectively.

Define the following bounds:

$$\alpha^+ = \alpha + \Delta\alpha \tag{23}$$

$$\alpha^- = \alpha - \Delta\alpha \tag{24}$$

$$\beta^+ = \beta + \Delta\beta \tag{25}$$

$$\beta^- = \beta - \Delta\beta \tag{26}$$

According to Eq. (22), K_s is simply calculated by:

$$K_s = \alpha \exp \beta \tag{27}$$

It should be noted that the errors made on the intercept β and the slope α cannot be considered as independent. Indeed, if the slope is overestimated for example, the intercept is very likely to be overestimated also (since h_f values are in the negative domain of the abscissa axis). Consequently, the location error made on K_s estimates is maximized by the product operation between α and β. There is no analytical expression for the error of the product of variables affected by non-independent errors. Thus, only the following bounds can be obtained:

$$K_s^+ = \alpha^+ \exp \beta^+ \tag{28}$$

$$K_s^- = \alpha^- \exp \beta^- \tag{29}$$

The location error on K_s is log-normally distributed and characterized by a factor f defined by:

$$f = \sqrt{\frac{K_s^+}{K_s^-}} \tag{30}$$

with:

$$K_s^- = K_s/f \leq K_s \leq K_s^+ = fK_s \tag{31}$$

3. Materials and methods

Millet crops and fallow grasslands covers are found, on sandy soils, all over the East Central Super Site of the HAPEX-Sahel experiment, except on the plateaus. Thus, they represent the main soil feature to be considered in the study of the biosphere–atmosphere interactions and their hydrodynamic characterization is essential for modeling purposes (Braud et al., 1997). Millet and fallow soils are subject to crusting (Casenave and Valentin, 1989). In non-crusted areas, soil can be considered to be vertically homogeneous.

The tiger bush, covering lateritic plateaus is characterized by a sandy-loamy-clay soil with a small hydraulic conductivity, producing high values of runoff, increased by the existence of large crust-covered areas separating vegetative strips. During the rainy season (June–September 1993), two types of crust, structural (ST) and sedimentation (SED), were selected for their spatial representativity and their ease of identification. The former can be found downslope of the vegetative strips and are formed by the sieving effect of raindrop impacts which concentrate fine particles at the basis of the structure with sand on top. Gravels are frequently included at the surface (type ST3, following the classification proposed by Valentin and Bresson, 1992). SED crusts, abundant in zones of accumulation of water, are found upslope of the vegetative strips and are formed by sedimentation of particles in small pools after rainfall events. Detailed description and analysis of Sahelian soil crusting is given in Casenave and Valentin (1989) and Valentin and Bresson (1992). Infiltration tests were also performed on the underlying soil to estimate difference in

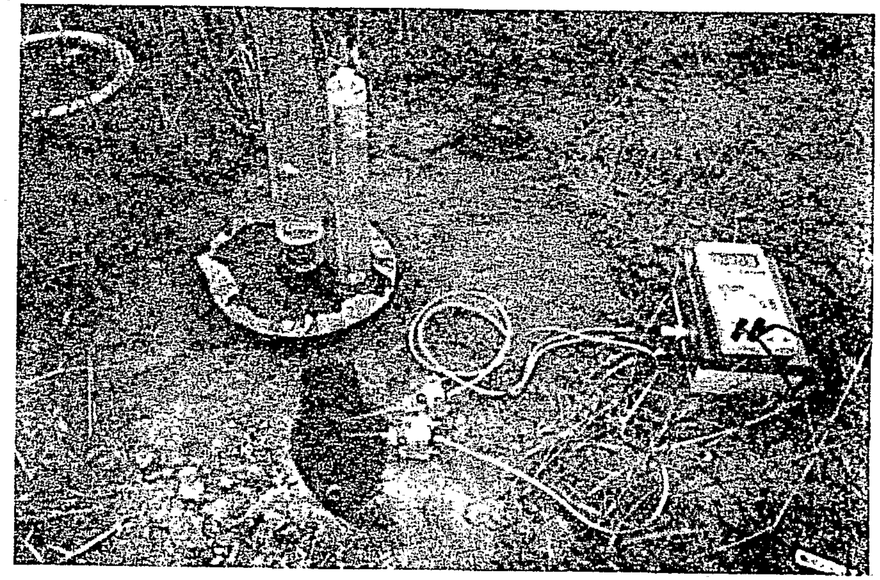

Fig. 1. Fallow grassland: disc infiltrometer D1 (left) and soil water pressure monitoring (here at two depths) with the pressure transducers (middle) connected to the alimentation and the voltmeter (right).

conductivity between crust and subsoil. For the tiger bush tests, initial volumetric water content was always lower than 5%, with an average of 1.9%.

Infiltration tests were carried out during two consecutive summers (1992 and 1993) with disc infiltrometers of 125 (D1) and 40 mm (D2) radius (Thony et al., 1991; Vauclin and Chopart, 1992). To monitor the time evolution of the soil water pressure, a minitensiometer (20 mm length, 2.2 mm diameter) connected to a pressure transducer (Data Instruments, Lexington, MA, USA) through a capillary tubing (1.45 mm internal diameter), was inserted horizontally under the disc at a depth ranging from 1 cm for crusted soils to 5 cm for sandy non-crusted soils. An overall view of the equipment is presented in Fig. 1.

In the millet fields and fallow sites (85% sand) infiltration tests were performed until a steady state flow condition was attained. While tests on millet plots were done between the plants, tests on fallow plots were carried out after removing about 1 cm of soil and cutting the above-ground vegetative cover while leaving the roots in place. The multi-radii method was used with $h_i = -10$, 40, 70, and 100 mm of water, with three replications for both discs, representing together a total of 48 tests. For each test, measurement of initial and final water content, performed by taking disturbed gravimetric samples, allowed determination of corresponding sorptivity and matric flux potential values (Eq. (12)) and comparison of steady state and transient analyses results. The single-radius multiple-potential method (Reynolds and Elrick, 1991; Ankeny et al., 1991), was also used for comparison.

In the tiger bush, the minitensiometer was installed only under the large disc infiltrometer (D1) because of a lower relative disturbance of soil. Moreover, the sorptivity

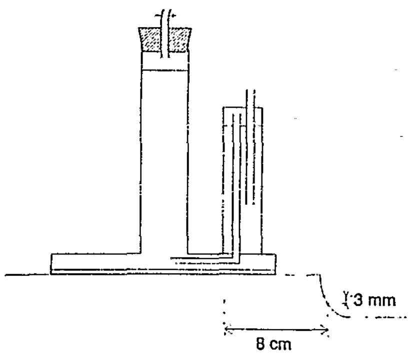

Fig. 2. Schematic implementation outline of the minitensiometer.

estimation with the small disc infiltrometer (D2), is quite inaccurate as the first term at right-hand side in Eq. (5) becomes relatively small as the radius decreases (see Eq. (6)). Thus, the sorptivity estimations used for this study were all obtained with D1. Because of the fragility of the crusts, the minitensiometer cannot be installed in dry conditions without the risk of significant soil disturbance (detachment, fracture, or cracking). Consequently, it was necessary to drill a hole into the soil, while injecting by small increments a total of about 1 cm^3 of water with a syringe. Installation of the tensiometer into this hole and infiltration test were performed 24 h later when the soil has dried. The porous cup was inserted at about 1 cm depth (its exact depth was measured after the test), at about mid-distance between the center and the edge of the disc (Fig. 2). Fig. 3 shows the mini-tensiometer under a SED crust after an infiltration test.

A ring of the same radius as the disc infiltrometer was placed on the soil surface and sand was placed in it and leveled. The quantity of sand was measured to estimate I_0 in Eq. (8) and t_0 in Eq. (11). The disc infiltrometer was then placed on this bed of sand and the cumulative infiltration was monitored. During infiltration, the tensiometer response to the arrival of the vertical wetting front, defined by the maximum of $\partial h/\partial t$, facilitates restricting the analysis to the stage corresponding to the crust only. At that moment (t_1) the progression of the lateral wetting front at the surface was also measured to estimate the ratio, I_{1d}/I_{3d}.

In order to quantify the deficit of moisture in the subsoil due to the crust impeding effect, infiltration tests were continued after t_1, until the tensiometer showed an approximately constant soil water pressure. At the end of every test, disturbed soil samples were taken at two depths and also around the disc for determination of final gravimetric water content. Two sampling operations were systematically performed, with about 30 s interval, so that the effect of the delay of sampling after the removal of the disc could be estimated (a decrease of about 0.01 g g^{-1} was found).

Gravimetric water contents were converted into volumetric values through dry bulk density (ρ_d) measured from undisturbed samples collected at the end of the season, following the method proposed by Fies and Zimmer (1982). Due to the impossibility to take undisturbed samples of ST crusts, a value of 1.7 g cm^{-3} was calculated by assuming a

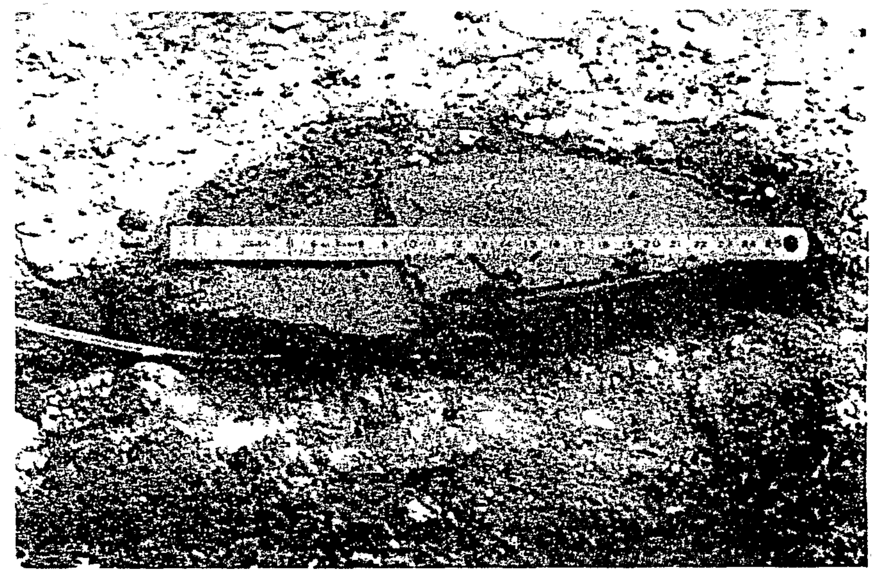

Fig. 3. Tiger bush, sedimentation crust: the inserted micro-tensiometer after removing half of the infiltrated zone at the end of a test. Note the sand contact layer partially unremoved (right).

specific density of 2.65 for the solids and assuming that measured saturated gravimetric water content represents 85% of porosity (this percentage was obtained from other crust types). However, this is a minor uncertainty compared with other sources of error.

In the tiger bush, 59 infiltration tests were performed with the disc D1, including 20 on ST crusts, 23 on SED crusts, and 16 on the underlying soil.

4. Results and discussion

4.1. Homogeneous soils: fallow and millet

For the fallow grassland, sorptivity and matric flux potential estimates obtained by Eqs. (11) and (12), respectively, are shown in Fig. 4, together with the $\Phi(h)$ curve obtained by fitting Eq. (14) to the data. Its derivative ($K(h)$) is plotted against results from steady state methods in Fig. 5, which shows the good agreement between all the methods for the fallow. Both multi-radii and multi-potential experiments exhibit a shift in conductivity near saturation. This change of the general slope, at about −20 mm, is characteristic of a change in functional pore size. The α values, about 10 m^{-1} for $h < -20$ mm and 40 m^{-1} for $h > -20$ mm, corresponds to pore radii of 80 and 330 μm, respectively. We attribute the shift to larger functional pore size to the influence of grass roots. This shift does not appear with the transient method result, which uses a single exponential function for the

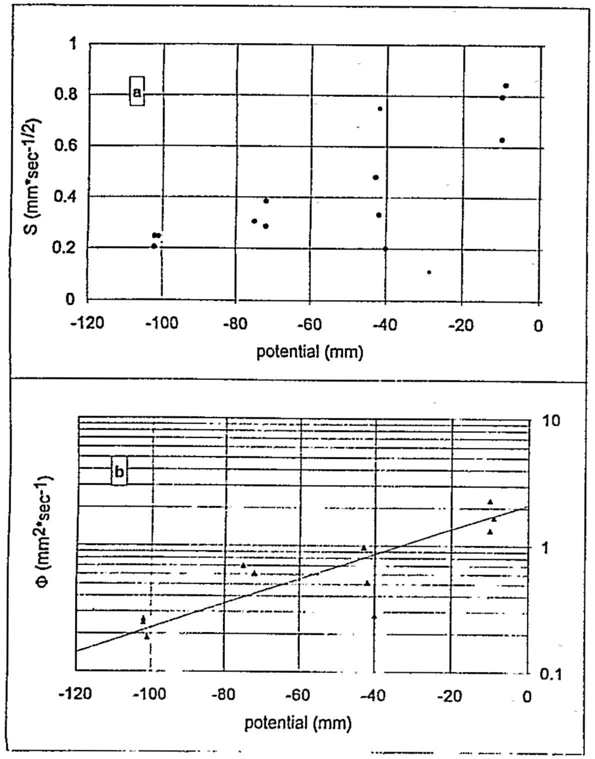

Fig. 4. Fallow grasslands: (a) sorptivity and (b) matric flux potential calculated (Eq. (12), triangles) and fitted (Eq. (14), continuous line), as a function of supply water potential.

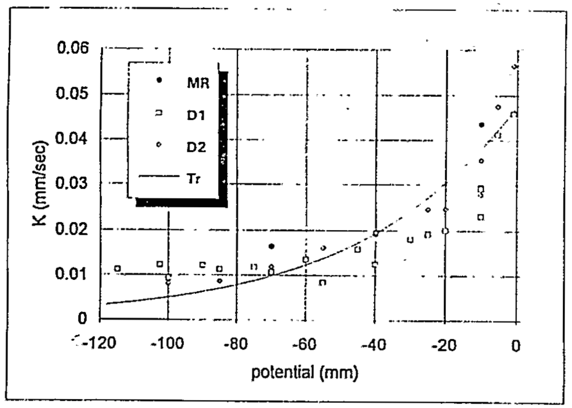

Fig. 5. Fallow grasslands: hydraulic conductivity as a function of water potential, by multi-radii analysis (MR), multi-potential analyses with the large (D1) and the small (D2) discs and transient analysis (Tr).

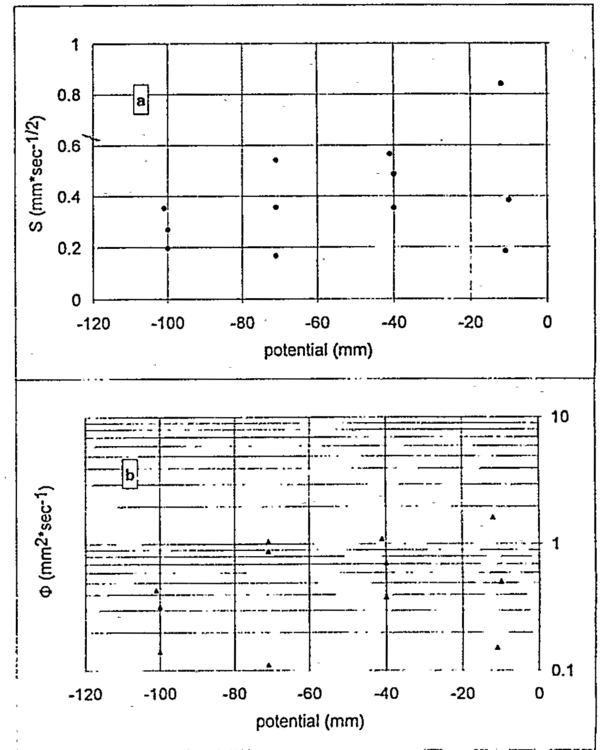

Fig. 6. Millet fields: (a) sorptivity and (b) matric flux potential, as a function of water potential.

whole domain. However, it is remarkable that the 'transient' α, 22 m^{-1} corresponds to a good mean value and that K_s is almost unchanged (Fig. 5).

For the millet cover, the transient method was found to be inadequate due to the high spatial variability of S. Indeed, the effects of localized working of the soil act to increase the infiltration flux only for part of the tests. Peugeot et al. (1997) found that these effects may persist up to 80 mm of rainfall. The slope of Φ versus h (Fig. 6(b)) cannot be estimated with reasonable accuracy, since the effects of spatial variability dominate those of supply potentials. In such a case, the differentiation operation becomes hazardous and thus, it is unrealistic to expect a correct estimation of conductivity. Consequently, the transient method should not be applied in the case of a high field heterogeneity, unless a very large number of tests is performed.

4.2. *Crusted soils: tiger bush*

4.2.1. *Infiltration*

Fig. 7 shows, for a typical infiltration test carried out at $h_f = -10$ mm of water on a ST crust, measured cumulative infiltration and soil water pressure as a function of time

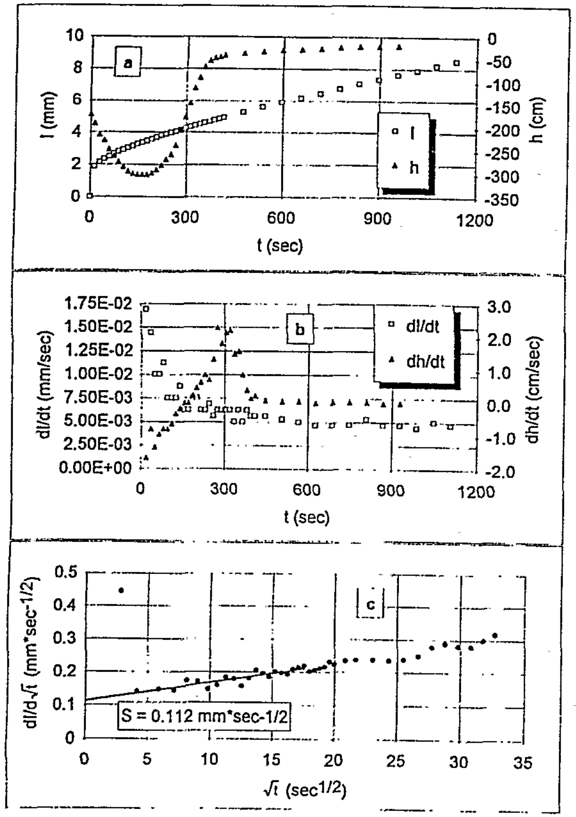

Fig. 7. Tiger bush, infiltration test at $h_f = -10$ mm: (a) measured cumulative infiltration depth (I) and soil water pressure (h); (b) infiltration flux (dI/dt) and soil water pressure variation with time (dh/dt); (c) sorptivity estimation by Eq. (11).

(Fig. 7(a)), the corresponding derivatives with time (Fig. 7(b)) and the sorptivity value obtained by using Eq. (11) (Fig. 7(c)). The early decrease in h is explained by the initial non-equilibrium of the tensiometer with its soil environment. Indeed, as soon as the porous cup is in contact with the dry soil (that is, a few minutes before the infiltration test begins), the water pressure decreases sharply to reach equilibrium with the low soil water potential. To avoid loosing the hydraulic contact between the porous surface and the soil, the infiltration test should be performed as quickly as possible after installing the tensiometer.

It can be noted that the final value of h does not correspond to the pressure applied, because of the well-known moisture deficit of the subsoil due to the impeding effect of the crust (Aboujaoudé et al., 1991; Touma, 1992). The measured value of h is an intermediate value between the water pressures in the crust and the subsoil which are not necessarily equal. The wetting front arrival can be identified at $t_1 = 300$ s (maximum of $\partial h/\partial t$, as seen in Fig. 7(b)). Thus, the cumulative infiltration data after 300 s are not considered in the

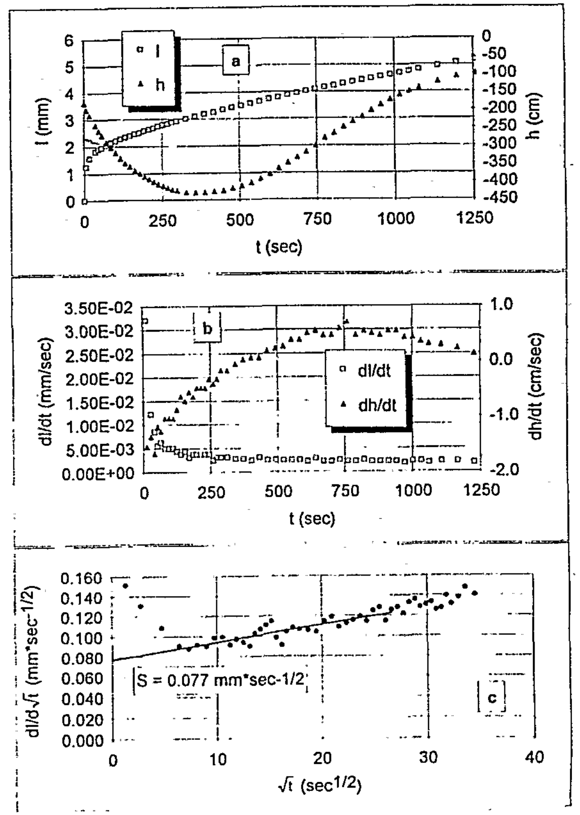

Fig. 8. Tiger bush, infiltration test at $h_f = -100$ mm: (a) measured cumulative infiltration depth (I) and soil water pressure (h); (b) infiltration flux (dI/dt) and soil water pressure variation with time (dh/dt); (c) sorptivity estimation by Eq. (11).

regression analysis of Eq. (11) to estimate sorptivity. The obvious early influence of the sand layer is revealed by the first point of Fig. 7(c) which falls far away from the linear behavior of the plotted data.

Similar graphs corresponding to another infiltration test carried out at $h_f = -100$ mm of water (Fig. 8) show a smoother response of the tensiometer, decreasing the accuracy of the t_1 estimate (about 750 s), both smaller flux and sorptivity, and a longer sand influence (about 25 s as seen in Fig. 8(c)). The inaccuracy on t_1 has obviously a large influence on the precision of S_1 estimates (see Eq. (19)), but its effect on S is small.

Measurements of lateral wetting front advance, both at t_1 and at the end of infiltration, showed an accentuated anisotropy of the wetting zone since the ratio of the lateral to the vertical front was found to be about 3.5 for ST and 2.6 for SED. This is probably one of the reasons why classical steady state methods lead to negative values of K for layered soils. It should be noted that our method avoided the effect of soil anisotropy

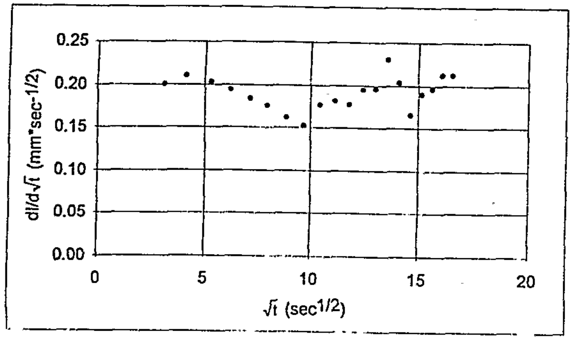

Fig. 9. Tiger bush: infiltration test rejected for sorptivity determination (Eq. (11)).

since only the intercept and not the slope of Eq. (11) is being analyzed. However, the method is flexible enough to account for anisotropy through the parameter B in Eqs. (5) and (11).

When infiltration data are plotted according to Eq. (11), the linearity is essential for sorptivity determination. Correlation coefficients higher than to 0.95 were commonly obtained, but in 35% of the cases, a curved behavior led to rejection of the results for Φ calculations. We suspect that the reason for which some of the experiments do not exhibit good linearity is related to the excessively large amount of sand required for situations with high surface roughness. Indeed, when a thick layer of sand is present between the disc and the soil, it is difficult to determine the number of early readings which should be rejected for sorptivity determination. As a matter of fact, the transition moment from infiltration into the sand layer to infiltration into the soil, is then difficult to see because of overlap between the two phenomena. This is illustrated in Fig. 9 which corresponds to a rejected test.

No significant difference was found between results for soil underlying ST crusts and soil underlying SED crusts. Fig. 10 presents the $\log_e\Phi$ versus h_f data for the three categories, ST, SED, and subsoil (SUB). The correct linearity which appears, despite the important scatter due to the use of squared S values, validates the choice of the exponential form (Eqs. (1) and (14)). Values of the different hydraulic parameters are summarized in Table 1. As shown in Peugeot et al. (1997), the K_s values obtained here for the crusts are quite consistent with the results of Casenave and Valentin (1992) who measured, in initially wet conditions and on the same crust types, critical values of rainfall intensity below which runoff does not occur.

Table 1
Tiger bush: hydraulic parameters for structural (ST) and sedimentation (SED) crusts and for the subsoil (SUB)

	ρ_d (g cm^{-3})	θ_s (cm^3 cm^{-3})	K_s (mm s^{-1})	S (mm s$^{-1/2}$)	α (mm^{-1})	λ_m (μm)	t_{grav} (h)
ST	1.7	0.31	$8.5e-4$	0.18	0.014	105	13
SED	1.47	0.35	$5.2e-4$	0.15	0.015	115	22
SUB	1.56	0.34	$2.8e-3$	0.27	0.023	175	2.5

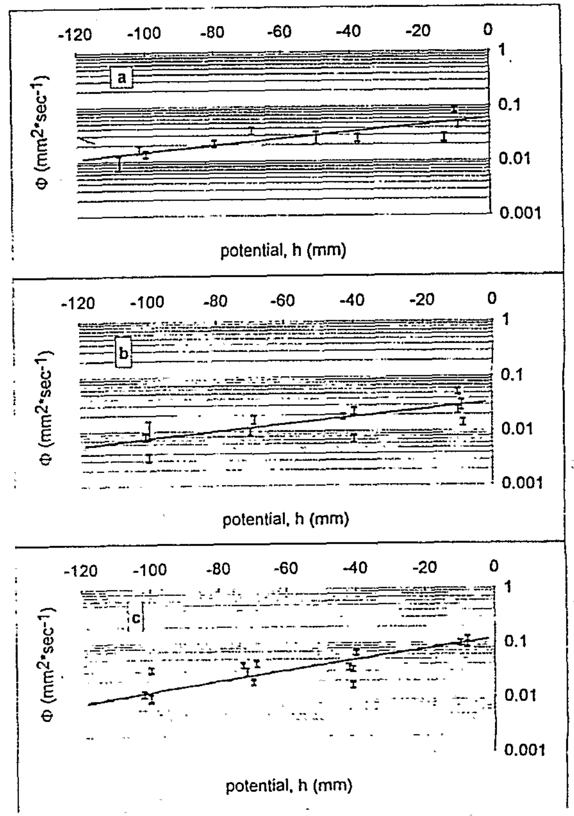

Fig. 10. Tiger bush, matric flux potential calculated (Eq. (12), bars) and fitted (Eq. (14), continuous line) as a function of water potential: (a) structural crusts, (b) sedimentation crusts, (c) subsoil. Error bars correspond to Eq. (20).

4.2.2. *Error analysis*

The ratio dS/S, given by the regression analysis (Eq. (11)) performed for each infiltration test, varies between 0.013 and 0.28 with a mean value of 0.056. This error is of the same order of magnitude as the error due to the use of the approximate value of 0.55 for the parameter b. Finally, Eq. (20) gives a mean relative error of about 20% for the matric flux potential estimates. The corresponding error bars are shown in Fig. 10.

Parameters of the location error analysis on K_s estimates (Eqs. (22)–(31)) are summarized in Table 2 for ST, SED, and SUB. The location error factor, ranging from 1.6 to 1.8, shows that spatial variability has the larger effect on the uncertainty of K_s estimates. This means that, to improve the global accuracy of the method, it is more important to increase the number of replications, than to perform a more accurate S determination for each test. Taking into account location error and error of Φ estimates, the global error made in K_s determination is log-normally distributed with a standard deviation of a factor $\pm$ 2.

Table 2

Tiger bush: parameters of the location error analysis (Eqs. (22)–(31)) for structural (ST) and sedimentation (SED) crusts and for the subsoil (SUB)

	ST	SED	SUB
β^+	−2.66	−3.25	−2.05
β^-	−3.12	−3.76	−2.56
α^+ (mm^{-1})	0.017	0.019	0.023
α^- (mm^{-1})	0.010	0.010	0.015
K_s^+ ($mm\ s^{-1}$)	1.2e−3	7.3e−4	2.9e−3
K_s^- ($mm\ s^{-1}$)	4.6e−4	2.4e−4	1.1e−3
f	1.61	1.75	1.61

Mohanty et al. (1994) carried out a spatial analysis of hydraulic conductivity measured using disc infiltrometers and obtained coefficients of variation for K_s between 75% and 125%. Thus, the error that we obtain here for K_s can be considered reasonable.

4.2.3. Characteristic length and time scales

The characteristic mean pore size λ_m (see Table 1), calculated by Eq. (15), with a precision of 30% (see Table 2), shows a decrease of 40% between subsoil and crust. These values were compared with results obtained by the mercury porosimetry technique (Fies, 1992a) on samples collected at the same place where the infiltration tests were performed. Fies showed that the porosity is bi-modal: one domain, characteristic of the clay fraction, has a pore size ranging from 10^{-2} to 10^{-1} μm. The second domain, with values ranging from 1 μm to a maximum value of 40 μm for ST and SED crusts and 100 μm for the subsoil, characterizes the coarse fraction (Fies, 1992b). Our field values of λ_m (110 μm for ST and SED, 175 μm for SUB, Table 1) appear markedly superior to laboratory measured maximum pore radius, which is in agreement with general findings reported by White and Sully (1987). Not surprisingly, our results illustrate the predominant hydraulic role of the coarse porosity on infiltration.

Estimation of t_{grav} (Table 1) by Eq. (16) shows that gravity effects can be neglected during at least 1 h of infiltration into a crust, which makes possible the use of Eq. (19) to obtain a second sorptivity estimate, S_1. S values, obtained by Eq. (11), are plotted against S_1 in Fig. 11, for tests providing the two estimates without any ambiguity. As no consistent underestimation appears in S_1 compared with S values, no water blockage effect is shown at the crust–soil interface. Indeed, such a phenomena would have entailed a delay in the tensiometer response to the wetting front arrival and thus decrease S_1 values. Therefore, it seems that ST and SED crusts can be effectively seen, from a hydrodynamic point of view, simply as impeding layers, by having a lower hydraulic conductivity than the subsoil.

Crust conductivity values obtained by this method were used in a soil–vegetation–atmosphere–transfer model (Braud et al., 1997) and led to improve the prediction of the soil water content as compared with measurements performed during the HAPEX-Sahel experiment. Results presented here for the tiger bush will be used to compute cumulative infiltration to predict pointwise runoff amounts for natural rainfall conditions and compare them with measured values obtained by Peugeot et al. (1997).

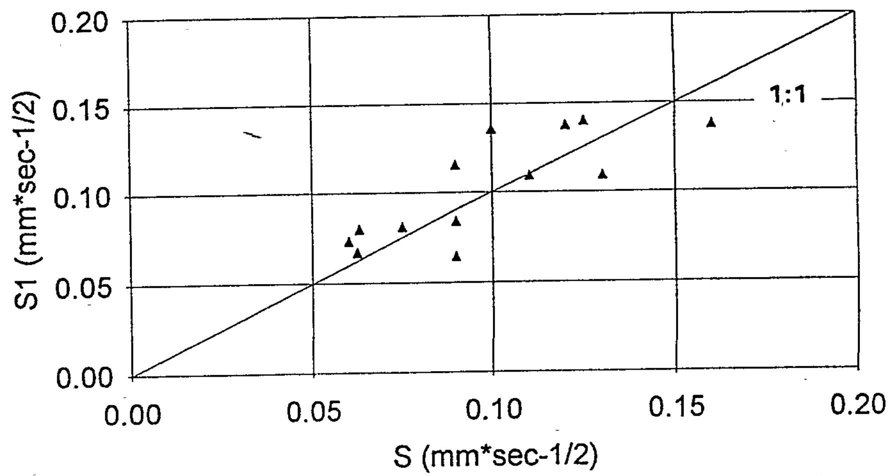

Fig. 11. Comparison of S (Eq. (11)) and S_1 (Eq. (19)) sorptivity estimates for structural and sedimentation crusts.

5. Conclusions

Faced with the inability of classical tension disc infiltrometry methods, based on the analysis of steady state regime of infiltration, to provide conductivity estimates of crusted soils, a new method has been developed, using transient flow analysis and minitensiometer implemented below the crust. Saturated hydraulic conductivity, obtained with a precision of a factor 2, decreased in the crust from three-fold to six-fold compared with the subsoil. The effective pore size was found to be significantly reduced by the crust formation and consistent with porosimetry measurements. The method would be particularly suitable for sandy crusts, for which the decrease in conductivity must be more accentuated. It is not recommended to use the method where crusts either have a high surface roughness (because of the need for a thick layer of sand) or are thinner than 1 cm (because of the difficulty of placing the minitensiometer at the crust–subsoil interface). More generally, the method could be used for any case of layered soils, the extra effort required for minitensiometers installation being largely offset by avoiding the steady state flow requirement.

Acknowledgements

The experimental part of this work, funded by CNRS (PIR Environnement) and INSU/CNRS (PAMOS), could not have been possible without the technical support of ORSTOM Niamey, Niger. Density measurements were performed at the Soil Science Department of INRA Avignon with the precious collaboration of Jean-Claude Fies. The first author wishes to thank Randel Haverkamp (LTHE Grenoble) and Brent Clothier (HortResearch, CRI Palmerston, New Zealand) for helpful discussions.

References

Aboujaoudé, A., Belleudy, P. and Vauclin, M., 1991. A numerical study of infiltration through crusted soils: flat and other surface configurations. Soil Tech., 4: 1–18.

Ahuja, L.R., 1974. Applicability of the Green–Ampt approach to water infiltration through surface crust. Soil Sci., 118: 283–288.

Ankeny, M.D., Ahmed, M., Kaspar, T.C. and Horton, R., 1991. Simple field method for determining unsaturated hydraulic conductivity. Soil Sci. Soc. Am. J., 55: 467–470.

Braud, I., Bessemoulin, P., Monteny, B., Sicot, M., Vandervaere, J.-P. and Vauclin, M., 1997. Unidimensional modeling of a fallow savannah during the HAPEX-Sahel experiment using the SiSPAT model. J. Hydrol., this issue.

Bristow, K.L. and Savage, M.J., 1987. Estimation of parameters for the Philip two-term infiltration equation applied to field soil experiments. Aust. J. Soil Res., 25: 369–375.

Casenave, A. and Valentin, C., 1989. Les États de Surface de la Zone Sahélienne. Ed. de l'ORSTOM, pp. 65–74.

Casenave, A. and Valentin, C., 1992. A runoff capability classification system based on surface features criteria in semi-arid areas of West Africa. J. Hydrol., 130: 231–249.

Clothier, B. and White, I., 1981. Measurement of sorptivity and soil water diffusivity in the field. Soil Sci. Soc. Am. J., 45: 241–245.

Cook, F.J. and Broeren, A., 1994. Six methods for determining sorptivity and hydraulic conductivity with disk permeameters. Soil Sci., 157: 2–11.

Elrick, D.E. and Robin, M.J., 1981. Estimating the sorptivity of soils. Soil Sci., 132: 127–133.

Fies, J.-C., 1992a. Mesures de conductivité hydrique de croûtes. Rapport Hapex Sahel/Niger, INRA internal report, 11 pp.

Fies, J.-C., 1992b. Analysis of soil textural porosity relative to skeleton particule size, using mercury porosimetry. Soil Sci. Soc. Am. J., 56: 1062–1067.

Fies, J.-C. and Zimmer, D., 1982. Effect of pressure on some characteristics of packing void in a sandy-clay material. Milieux poreux et transferts hydriques. Bull. du Groupe Français d'Humidimétrie Neutronique, Ed. CEMAGREF, Aix-en-Provence, France, 12: 39–54 (in French).

Gardner, W.R., 1958. Some steady-state solutions of the unsaturated moisture flow equation with application to evaporation from a water table. Soil Sci., 85: 228–232.

Goutorbe, J.-P., Lebel, T., Tinga, A., Bessemoulin, P., Brouwer, J., Dolman, A.J., Engman, E.T., Gash, J.H.C., Hoepffner, M., Kabat, P., Monteny, B.A., Prince, S., Said, F., Sellers, P. and Wallace, J.S., 1994. Hapex-Sahel: a large scale study of land–atmosphere interactions in the semi-arid tropics. Ann. Geophysicae, 12: 53–64.

Haverkamp, R., Ross, P.J., Smettem, K.R.J. and Parlange, J.Y., 1994. Three-dimensional analysis of infiltration from the disc infiltrometer. 2. Physically based infiltration equation. Water Resour. Res., 30: 2931–2935.

Hillel, D. and Gardner, W.R., 1969. Steady infiltration into crust-topped profiles. Soil Sci., 108: 137–142.

Hillel, D. and Gardner, W.R., 1970. Transient infiltration into crust-topped profiles. Soil Sci., 109: 69–76.

Hoogmoed, W.B. and Stroosnijder, L., 1984. Crust formation on sandy soils in the Sahel. I. Rainfall and infiltration. Soil Tillage Res., 4: 5–23.

Hussen, A.A. and Warrick, A.W., 1993. Alternative analyses of hydraulic data from the disc tension infiltrometers. Water Resour. Res., 29: 4103–4108.

Logsdon, S.D. and Jaynes, D.B., 1993. Methodology for determining hydraulic conductivity with tension infiltrometers. Soil Sci. Soc. Am. J., 57: 1426–1431.

Mohanty, B.P., Ankeny, M.D., Horton, R. and Kanwar, R.S., 1994. Spatial analysis of hydraulic conductivity measured using disc infiltrometers. Water Resour. Res., 30: 2489–2498.

Parlange, J.Y., 1972. Theory of water movement in soils: 4. Two and three dimensional steady infiltration. Soil Sci., 113: 96–101.

Parlange, J.Y., Hogarth, W.L. and Parlange, M.B., 1984. Optimal analysis of a surface crust. Soil Sci. Soc. Am. J., 48: 494–497.

Perroux, K.M. and White, I., 1988. Design for disc permeameters. Soil Sci. Soc. Am. J., 52: 1205–1215.

Peugeot, C., Estèves, M., Rajot, J.-L., Vandervaere, J.-P. and Galle, S., 1997. Runoff generation processes: results and analysis of field data collected at the East Central Super Site of the HAPEX-Sahel experiment. J. Hydrol., this issue.

Philip, J.R., 1957. The theory of infiltration: 4. Sorptivity and algebraic infiltration equations. Soil Sci., 84: 257–264.

Philip, J.R., 1969. Theory of infiltration. Adv. Hydrosci., 5: 215–296.

Philip, J.R., 1987. The quasilinear analysis, the scattering analog and other aspects of infiltration and seepage. In: Y.-S. Fok (Editor), Infiltration Development and Application. Water Resources Research Center, Honolulu, Hawaii, pp. 1–27.

Quadri, M.B., Clothier, B.E., Angulo Jaramillo, R., Vauclin, M. and Green, S.R., 1994. Axisymmetric transport of water and solute underneath a disk permeameter: experiments and numerical model. Soil Sci. Soc. Am. J., 58: 696–703.

Reynolds, W.D. and Elrick, D.E., 1991. Determination of hydraulic conductivity using a tension infiltrometer. Soil Sci. Soc. Am. J., 55: 633–639.

Scotter, D.R., Clothier, B.E. and Harper, E.R., 1982. Measuring saturated hydraulic conductivity and sorptivity using twin rings. Aust. J. Soil Res., 20: 295–304.

Sharma, M.L., Gander, G.A. and Hunt, C.G., 1980. Spatial variability of infiltration in a watershed. J. Hydrol., 45: 101–122.

Smettem, K.R.J. and Clothier, B.E., 1989. Measuring unsaturated sorptivity and hydraulic conductivity using multiple disc permeameters. J. Soil Sci., 40: 563–568.

Smiles, D.E. and Harvey, A.G., 1973. Measurement of moisture diffusivity in wet swelling systems. Soil Sci., 116: 391–399.

Smiles, D.E. and Knight, J.H., 1976. A note on the use of the Philip infiltration equation. Aust. J. Soil Res., 14: 103–108.

Smiles, D.E., Knight, J.H. and Perroux, K.M., 1982. Absorption of water by soil: the effect of a surface crust. Soil Sci. Soc. Am. J., 46: 476–481.

Talsma, T., 1969. In situ measurement of sorptivity. Aust. J. Soil Res., 7: 269–276.

Thony, J.-L., Vachaud, G., Clothier, B.E. and Angulo-Jaramillo, R., 1991. Field measurement of the hydraulic properties of soil. Soil Tech., 4: 111–123.

Touma, J., 1992. Numerical simulation of infiltration into crusted soils: crust either established or under formation. Hydrol. Continent., Ed. ORSTOM, Paris, France, 7: 143–156 (in French).

Turner, N.C. and Parlange, J.-Y., 1974. Lateral movement at the periphery of a one-dimensional flow of water. Soil Sci., 118: 70–77.

Valentin, C. and Bresson, L.M., 1992. Morphology, genesis and classification of surface crusts in loamy and sandy soils. Geoderma, 55: 225–245.

Vauclin, M. and Chopart, J.-L., 1992. Multiple disk infiltrometers for field determination of surface hydraulic properties of a gravelly soil in Ivory Coast. Agron. Trop., 46: 259–271 (in French).

Warrick, A.W., 1992. Models for disc infiltrometers. Water Resour. Res., 28: 1319–1327.

Warrick, A.W. and Broadbridge, P., 1992. Sorptivity and macroscopic capillary length relationships. Water Resour. Res., 28: 427–431.

Warrick, A.W. and Lomen, D.O., 1976. Time-dependant linearized infiltration: III. Strip and disc sources. Soil Sci. Soc. Am. J., 40: 639–643.

White, I. and Perroux, K.M., 1989. Estimation of unsaturated hydraulic conductivity from field sorptivity measurements. Soil Sci. Soc. Am. J., 53: 324–329.

White, I. and Sully, M.J., 1987. Macroscopic and microscopic capillary length and time scales from field infiltration. Water Resour. Res., 23: 1514–1522.

Wooding, R.A., 1968. Steady infiltration from a shallow circular pond. Water Resour. Res., 4: 1259–1273.